World Academy of Science, Engineering and Technology
International Journal of Physical and Mathematical Sciences
Vol:6, No:12, 2012

A Transform-Free HOC Scheme for Incompressible Viscous Flow past a Rotationally Oscillating Circular Cylinder

Rajendra K. Ray, and H. V. R. Mittal

***Abstract*—**A numerical study is made of laminar, unsteady flow behind a rotationally oscillating circular cylinder using a recently developed higher order compact (HOC) scheme. The stream function vorticity formulation of Navier-Stokes (N-S) equations in cylindrical polar coordinates are considered as the governing equations. The temporal behaviour of vortex formation and relevant streamline patterns of the flow are scrutinized over broad ranges of two externally specified parameters namely dimensionless forced oscillating frequency S_f and dimensionless peak rotation rate α_m for the Reynolds's number Re = 200. Excellent agreements are found both qualitatively and quantitatively with the existing experimental and standard numerical results.

***Keywords*—**HOC, Navier-Stokes, non-uniform polar grids, rotationally oscillating cylinder.

I. Introduction

DURING last one decade Higher Order Compact (HOC) finite difference schemes have established themselves as potential numerical schemes in the field of Computational fluid Dynamics to study different aspects of fluid dynamics. Kalita et al. [1] first developed this type of HOC scheme on rectangular non-uniform grids for the steady 2D convection-diffusion equation with variable coefficients without any transformation. Later on, Ray and Kalita [2], [3] have extended the scheme for non-uniform polar grids which can be easily extended for curvilinear coordinates. The accuracy and reliability of this HOC scheme has already been ascertained in the case of flow past an impulsively started circular cylinder and its rotating counterparts [2]-[4]. Till now present scheme has not been tested for the complex flow problems where periodic rotary oscillation condition is used on the cylinder wall.

A literature survey reveals that though much of the earlier studies have been made in the case of a rotationally oscillating circular cylinder, both numerically and experimentally, but still there are many aspects to be clarified in this regard. The distinct feature of this rotatory oscillatory motion is that around the long axis, the moving surfaces perform an alternate periodic motion, which consists of an alternate acceleration and deceleration between the fixed angular amplitude.

In this present work, we extend the applicability of our newly developed scheme in reference [2] to capture the very complex flow phenomena of unsteady flow past a rotationally oscillating circular cylinder for the Reynolds numbers Re = 200 with different forced oscillating frequencies (S_f) and peak rotation rates (α_m). We compute the flow for very long duration of time to investigate the influence of S_f and α_m on vortex shedding phenomenon as well as lift and drag coefficients, Power spectra, etc. We compare the computed results, both qualitatively and quantitatively, with the experimental flow visualizations and numerical results that are available in the literature. In all the cases, our numerical results are in excellent agreement with the existing results.

The paper is arranged in the following way. In section II, we discuss about the mathematical formulation and discretization procedure, section III deals with our numerical results and comparisons with existing experimental and numerical results. Finally, in section IV, we summarize our observations in the conclusions.

II. Mathematical Formulation and Discretization Procedure

A. Governing Equations and Boundary Conditions

The flow is governed by the unsteady incompressible N-S equations. In non-dimensional form, the ψ-ω formulation of the 2D N-S equations in cylindrical polar coordinates (r, θ) are given by

$$\begin{aligned} &\frac{\partial^2\omega}{\partial r^2}+\frac{1}{r}\frac{\partial\omega}{\partial r}+\frac{1}{r^2}\frac{\partial^2\omega}{\partial\theta^2}=\mathrm{Re}\,(u\frac{\partial\omega}{\partial r}+\frac{v}{r}\frac{\partial\omega}{\partial\theta}+\frac{\partial\omega}{\partial t}) \\ &\frac{\partial^2\psi}{\partial r^2}+\frac{1}{r}\frac{\partial\psi}{\partial r}+\frac{1}{r^2}\frac{\partial^2\psi}{\partial\theta^2}=-\omega \end{aligned} \tag{1}$$

Here ψ is the stream function, ω the vorticity, u, v respectively are the radial and tangential velocity components, t is the time and $\mathrm{Re}=\frac{UD}{\nu}$ is the Reynolds's number with U being the characteristic velocity, D is the characteristic length (like the diameter of the a cylinder) and υ the kinematic viscosity. The velocities u and v in terms of ψ are given by

$$u=\frac{1}{r}\frac{\partial\psi}{\partial\theta}\ and\ v=-\frac{\partial\psi}{\partial r}, \tag{2}$$

Rajendra K. Ray is with the School of Basic Sciences, Indian Institute of Technology Mandi, Himachal Pradesh, India (e-mail: rajendra@iitmandi.ac.in).

H. V. R. Mittal is with the School of Basic Sciences, Indian Institute of Technology Mandi Himachal Pradesh, India (e-mail: mittal2988@gmail.com).

and the vorticity ω is given by $\omega=\frac{1}{r}[\frac{\partial}{\partial r}(vr)-\frac{\partial u}{\partial \theta}]$ (3)

To compute the flow, we have used our recently developed transformation-free HOC scheme [2] for the unsteady, incompressible N-S equations on non-uniform polar grids. This scheme, whose temporal discretization is analogous to Crank-Nicolson type, is second order accurate in time and at least third order accurate in space. To apply this scheme, we first construct a non-uniform finite-difference 181 × 181 grid in the annular region $\Omega = [R_o, R_\infty] \times [0, 2\pi]$. The grid points are clustered around the surface of the cylinder to capture the boundary-layer effect. Continuity conditions at θ = 0 and θ = 2π are taken as the boundary conditions along those two lines. At the (i, j^{th}) node, the forward and backward step lengths in the r-direction are given by $r_f = (r_{i+1} - r_i), r_b = (r_i - r_{i-1})$ respectively. Similarly in the θ-direction, $\theta_f = (\theta_{j+1} - \theta_j)$ $\theta_b = (\theta_j - \theta_{j-1})$. Thus the HOC finite difference approximation for (1) at the (i, j^{th}) node of the computational domain are given by

$$[A11_{i,j}\delta r^2 + A12_{i,j}\delta\theta^2 + A13_{i,j}\delta r + A14_{i,j}\delta\theta + A15_{i,j}\delta r\delta\theta + A16_{i,j}\delta r\delta\theta^2 + A17_{i,j}\delta r^2\delta\theta + A18_{i,j}\delta r^2\delta\theta^2]\omega_{i,j}^{n+1} = [A21_{i,j}\delta r^2 + A22_{i,j}\delta\theta^2 + A23_{i,j}\delta r + A24_{i,j}\delta\theta + A25_{i,j}\delta r\delta\theta + A26_{i,j}\delta r\delta\theta^2 + A27_{i,j}\delta r^2\delta\theta + A28_{i,j}\delta r^2\delta\theta^2]\omega_{i,j}^{n} \quad (4)$$

And

$$[B1_{i,j}\delta r^2 + B2_{i,j}\delta\theta^2 + B3_{i,j}\delta r + B4_{i,j}\delta r\delta\theta + B5_{i,j}\delta r\delta\theta^2 + B6_{i,j}\delta r^2\delta\theta + B7_{i,j}\delta r^2\delta\theta^2]\psi_{i,j}^{n} = G_{i,j} \quad (5)$$

respectively, where the coefficients are given by

$$B1_{i,j} = 1 - \frac{(r_f - r_b)}{2r_i} + (r_i H_{21} - H_{22})\frac{1}{r_i^2} - \frac{2H_{22}}{r_i^3},$$

$$B2_{i,j} = \frac{1}{r_i^2} - (r_i H_{21} - H_{22})\frac{2}{r_i^4} + \frac{2H_{22}}{r_i^3},$$

$$B3_{i,j} = \frac{1}{r_i} - (r_i H_{21} - H_{22})\frac{1}{r_i^3} + \frac{2H_{22}}{r_i^3},$$

$$B4_{i,j} = r_i K_{21},$$

$$B5_{i,j} = (r_i H_{21} - H_{22})\frac{1}{r_i^3} + \frac{4H_{22}}{r_i^3} + r_i K_{22},$$

$$B6_{i,j} = r_i^2 K_{21}, B7_{i,j} = \frac{H_{22}}{r_i^2} + r_i^2 K_{22},$$

$$G_{i,j} = -[1 + (r_i H_{21} - H_{22})\frac{1}{r_i}\delta r + H_{22}\delta r^2 + K_{21}\delta r^2\delta\theta + K_{22}\delta r^2\delta\theta^2]\omega_{i,j}.$$

and

$$A11_{i,j} = (H_{12}\,\mathrm{Re} - 0.5\Delta t A1_{i,j}), A21_{i,j} = (H_{12}\,\mathrm{Re} + 0.5\Delta t A1_{i,j}),$$

$$A12_{i,j} = (r_i^2 K_{12}\,\mathrm{Re} - 0.5\Delta t A2_{i,j}), A22_{i,j} = (r_i^2 K_{12}\,\mathrm{Re} + 0.5\Delta t A2_{i,j}),$$

$$A13_{i,j} = (\mathrm{Re}(H_{11} - c_1 H_{12}) - 0.5\Delta t A3_{i,j}),$$
$$A23_{i,j} = (\mathrm{Re}(H_{11} - c_1 H_{12}) + 0.5\Delta t A3_{i,j}),$$

$$A14_{i,j} = (r_i^2\,\mathrm{Re}(K_{11} + r_i\,\mathrm{Re}\,v_{i,j}K12) - 0.5\Delta t A4_{i,j}),$$
$$A24_{i,j} = (r_i^2\,\mathrm{Re}(K_{11} + r_i\,\mathrm{Re}\,v_{i,j}K12) + 0.5\Delta t A4_{i,j}),$$

$$A15_{i,j} = -0.5\Delta t A5_{i,j}, A25_{i,j} = 0.5\Delta t A5_{i,j},$$
$$A16_{i,j} = -0.5\Delta t A6_{i,j}, A26_{i,j} = 0.5\Delta t A6_{i,j},$$

$$A17_{i,j} = -0.5\Delta t A7_{i,j}, A27_{i,j} = 0.5\Delta t A7_{i,j},$$
$$A18_{i,j} = -0.5\Delta t A8_{i,j}, A28_{i,j} = 0.5\Delta t A8_{i,j},$$

where

$$A1_{i,j} = 1 - 0.5c_1(r_f - r_b) - (H_{12}c_1^2 - c_1 H_{11}) - 2H_{12}(\mathrm{Re}(u_r)_{i,j} + \frac{1}{r_i^2})$$

$$A2_{i,j} = \frac{1}{r_i^2} + 0.5d_1(\theta_f - \theta_b) - \frac{2}{r_i^3}(H_{11} - H_{12}c_1) + \frac{6H_{12}}{r_i^4} - \mathrm{Re}\,v_{i,j}r_i(K_{11} + \mathrm{Re}\,v_{i,j}r_i K_{12}) - 2K_{12}\,\mathrm{Re}(v_\theta)_{i,j}r_i,$$

$$A3_{i,j} = c_1(H_{11} - c_1 H_{12})(\mathrm{Re}(u_r)_{i,j} + \frac{1}{r_i^2}) - H_{12}(\mathrm{Re}(u_{rr})_{i,j} - \frac{2}{r_i^3}) - \mathrm{Re}(u_\theta)_{i,j}r_i^2(K_{11} + \mathrm{Re}\,v_{i,j}r_i K_{12}) - K_{12}\,\mathrm{Re}(v_{\theta\theta})_{i,j}r_i^2,$$

$$A4_{i,j} = -d_1 - (H_{11} - c_1 H_{12})((v_r)_{i,j}r_i - v_{i,j})\frac{\mathrm{Re}}{r_i^2} - H_{12}((v_{rr})_{i,j}r_i^2 - 2(v_r)_{i,j}r_i) + 2v_{i,j})\frac{\mathrm{Re}}{r_i^3} - \mathrm{Re}(v_\theta)_{i,j}r_i(K_{11} + \mathrm{Re}\,v_{i,j}r_i K_{12}) - K_{12}\,\mathrm{Re}(v_{\theta\theta})_{i,j}r_i,$$

$$A5_{i,j} = -d_1 - (H_{11} - c_1 H_{12}) - 2H_{12}((v_r)_{i,j}r_i - v_{i,j})\frac{\mathrm{Re}}{r_i^2} + c_1 r_i^2(K_{11} + \mathrm{Re}\,v_{i,j}r_i K_{12}) - 2K_{12}\,\mathrm{Re}(v_\theta)_{i,j}r_i^2,$$

$$A6_{i,j} = (H_{11} - c_1 H_{12})\frac{1}{r_i^2} - \frac{4H_{12}}{r_i^3} + c_1 K_{12}r_i^2,$$
$$A7_{i,j} = -d1H_{12} + r_i^2(K_{11} + \mathrm{Re}\,v_{i,j}r_i K_{12}),$$

$$A8_{i,j} = \frac{H_{12}}{r_i^2} + K_{12}r_i^2,$$

$$H_{11} = \frac{1}{6}\{2(r_f - r_b) + cr_f r_b\},$$

$$H_{12}=\frac{1}{24}\{2(r_f^2-r_b^2-r_f r_b)+cr_f r_b(r_f-r_b)\},$$

$$K_{11}=\frac{1}{6}\{\frac{2}{r_i^2}(\theta_f-\theta_b)+d\theta_f\theta_b\},$$

$$K_{12}=\frac{1}{24}\{\frac{2}{r_i^2}(\theta_f^2+\theta_b^2-\theta_f\theta_b)+d\theta_f\theta_b(\theta_f-\theta_b)\},$$

$$H_{21}=\frac{1}{6}\{2(r_f-r_b)+\frac{r_f r_b}{r_i}\},$$

$$H_{22}=\frac{1}{24}\{2(r_f^2-r_b^2-r_f r_b)+\frac{r_f r_b}{r_i}(r_f-r_b)\},$$

$$K_{21}=\frac{1}{3r_i^2}(\theta_f-\theta_b), K_{22}=\frac{1}{12r_i^2}(\theta_f^2+\theta_b^2-\theta_f\theta_b)$$

In order to solve the algebraic system of equations resulting from above discretisation, we have used the hybrid biconjugate gradient stabilised method BiCGStab without preconditioning.

The details of the discretization leading to equations (4) and (5) as well as those of the finite difference operators can be found in [2].

III. Numerical Results and Discussion

The outcomes of our scheme are found to be satisfactory for the two dimensional computations using a non-uniform polar grid of size (181 × 181) with clustering near the surface of the cylinder, along the radial direction. Such a grid can be generated with the help of the following stretching function

$$r_i=\exp(\frac{\lambda\pi i}{i_{\max}})$$

where λ determining the outer radius of the computational domain. The far field boundary is considered at a distance 15 times the radius of the cylinder and time step is fixed at 0.001. The rotation of the cylinder enters the boundary conditions in terms of non-dimensional speed α which can be expressed as $\alpha = \alpha_m \sin 2\pi S_e t$. Here S_e denotes dimensionless frequency ratio S_f/S_o and α_m is the dimensionless peak rotation rate. S_f is the forced oscillating frequency of the cylinder and S_o is the frequency of the vortex shedding for flow past a stationary cylinder. For a fixed Reynolds's number Re, α_m and S_f are employed as the main parameters. Typical values of S_f / S_o = 0.2 and 1.0 for α_m = 0.5 and 2.0 are taken, as numerical results are available in the literature for these values.

A. Flow Behavior at $\alpha_m = 0.5$

Fig. 1 depicts instantaneous streamlines plotted in a fixed frame for S_f/S_o = 0.2 and Re = 200 for a fully developed flow at four instants over one complete period of oscillation (T_f). This figure shows the almost periodic nature of the flow. This can be confirmed by the lift and drag coefficients. Fig 2(a) plots the lift and drag coefficients. But, from this figure one can see the existence of more than one frequency. This can be further confirmed by studying the power spectrum analysis of the corresponding lift coefficient in Fig. 2(b). Such a representation helps us to understand a physical process more closely. Fourier transform equations are used to relate the corresponding peaks of lift coefficients with frequency. Power spectral density analysis of lift coefficient confirms two shedding frequency peaks, out of them one is dominant and other one is weaker. These two frequency peaks can be explained as follows: the dominant peak corresponds to the forced oscillation frequency of the cylinder S_f and weaker one corresponds to the vortex shedding frequency denoted by S_v [5]. Our computed results are matching well with the corresponding results of Cheng et al. [5].

To study the effect of S_f, when increased, Fig. 3 clearly depicts the near wake topology when the cylinder is rotationally oscillating at a frequency S_f equal to the natural vortex shedding frequency S_o (i.e. S_f/S_o = 1.0) for Re = 200. The instantaneous streamlines contours are plotted for the fully developed flow at four equal instants of time during one complete period of oscillation. This figure shows the periodic nature of the flow.

This can be further confirmed by the lift and drag coefficients plotted in Fig. 4(a). Unlike Fig. 2(a), this figure shows only one frequency. The corresponding power spectra of the lift coefficient, plotted in Fig. 4(b) confirm one single peak which is basically the forced oscillating frequency peak S_f as described by Cheng et al. [5]. Our computed results are in good agreements with those of Cheng et al. [5].

B. Flow Behavior at $\alpha_m = 2.0$

Now we study the flow behaviour when α_m is as high as 2.0 with S_f/S_o = 0.2 and 1.0, same as the previous values at α_m = 0.5. Fig. 5 depicts instantaneous streamlines plotted for Re = 200 at S_f/S_o = 0.2 at four equal intervals of time for a complete period. From this figure one can see the repetitive nature of flow field in the near wake which is mirror resemblance of the respective streamlines. Fig. 6(a) plots the lift and drag coefficients. One can observe that there is an increase in the amplitude of fluctuation of both the lift and drag coefficients as compared to the previous case (i.e., S_f/S_o = 0.2 and α_m = 0.5). Corresponding power spectra is shown in Fig. 6(b). The figure shows one dominant peak for S_f along with a very small second peak for S_v. The same observations are recorded by Cheng et al. [5].

To show the further efficacy of our scheme, instantaneous vorticity contours are plotted for S_f/S_o = 1.0 in Fig. 7 at four equal intervals of time in one complete oscillation cycle. Typical values of these parameters are considered in order to validate our numerical results with the observations reported by Lu and Sato [6].

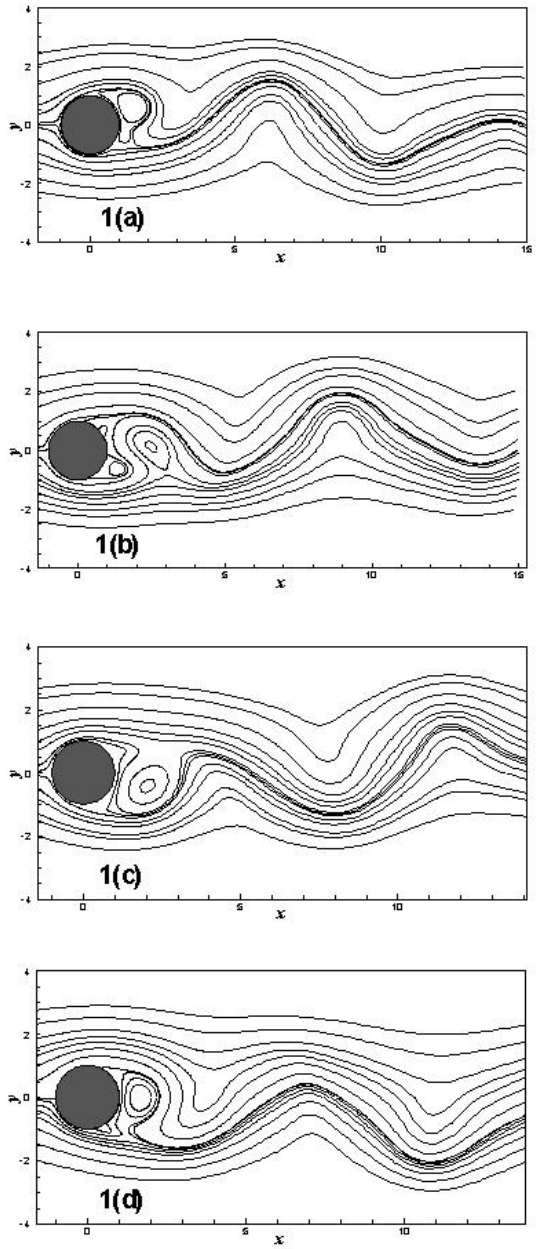

Fig. 1 Streamlines for Re = 200, S_f/S_o = 0.2 and α_m = 0.5, at t = (a) T_f/4, (b) T_f/2, (c) 3T_f/4, (d) T_f

Our results are in excellent agreement with those of Lu and Sato [6]. These contour plots depict that opposite sign vortices are shed from both sides of the cylinder in one complete oscillation cycle where positively and negatively oriented vortices are shown by solid and dotted lines respectively.

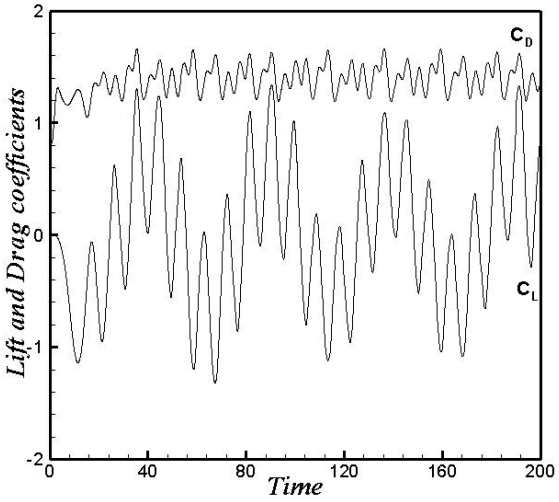

Fig. 2 (a) Lift and Drag coefficients for Re = 200, S_f/S_o = 0.2 and α_m = 0. 5

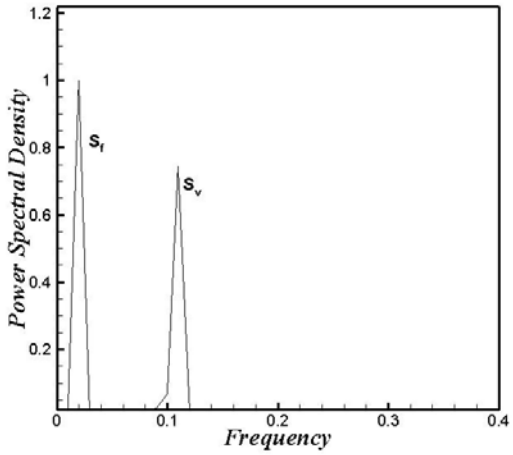

Fig. 2 (b) Power Spectra for Re = 200, S_f/S_o = 0.2 and α_m = 0. 5

One can clearly find that the flow is periodic in nature. Sinusoidal variation of lift and drag coefficient curves at a fixed amplitude in the superimposed lift and drag coefficient records in Fig. 8(a) discloses that vortex shedding from both sides of the cylinder is almost of same size and strength. The corresponding power spectra in Fig. 8(b) shows one single peak, which is justifying the Fig. 8(a).

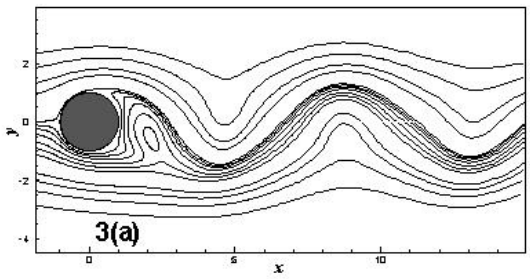

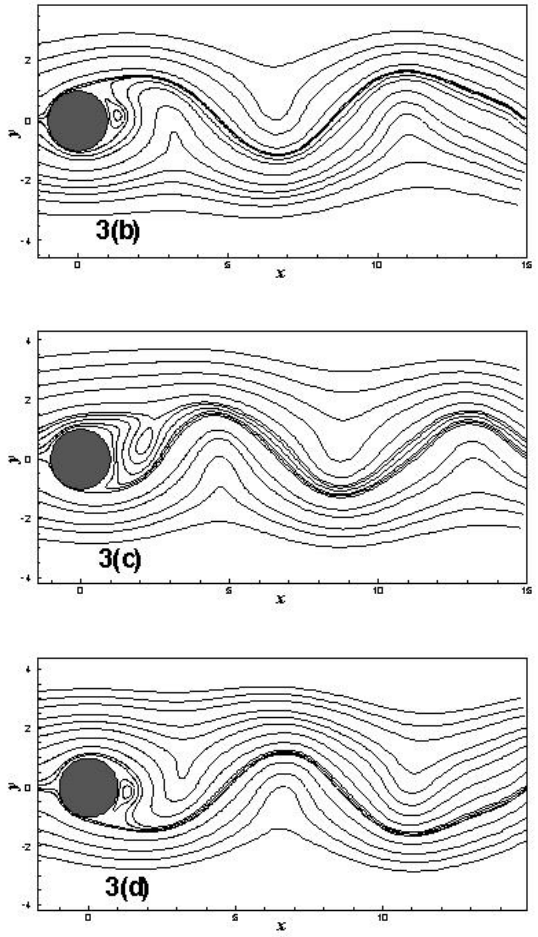

Fig. 3 Streamlines for Re = 200, S_f/S_o = 1.0 and α_m = 0.5, at t = (a) T_f /4, (b) T_f /2, (c) 3T_f /4, (d) T_f

IV. Conclusion

In this paper, we carry out a numerical investigation of the unsteady flow past rotationally oscillating circular cylinder for Reynolds numbers Re = 200 with S_f/S_o = 0.2, 1.0 and α_m = 0.5, 2.0, using a recently developed unsteady HOC scheme on non-uniform polar grid. We present detailed discussions of the effect of the parameters α_m and S_f on flow patterns. We observe that for each (α_m, S_f) combination, a periodic nature of the flow is seen. The power spectra of the flow shows double

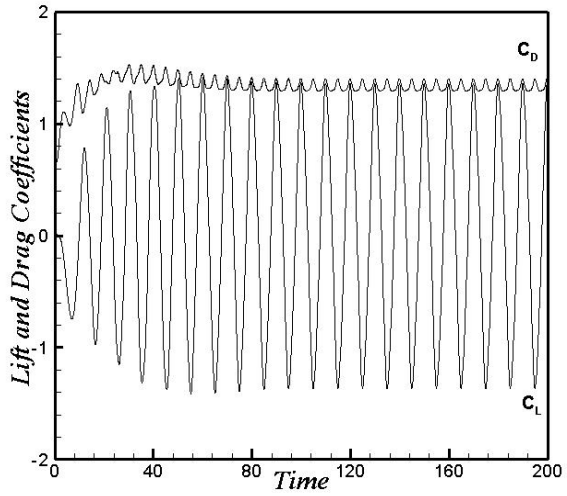

Fig. 4(a) Lift and Drag coefficients for Re = 200, S_f/S_o = 1.0 and α_m = 0. 5

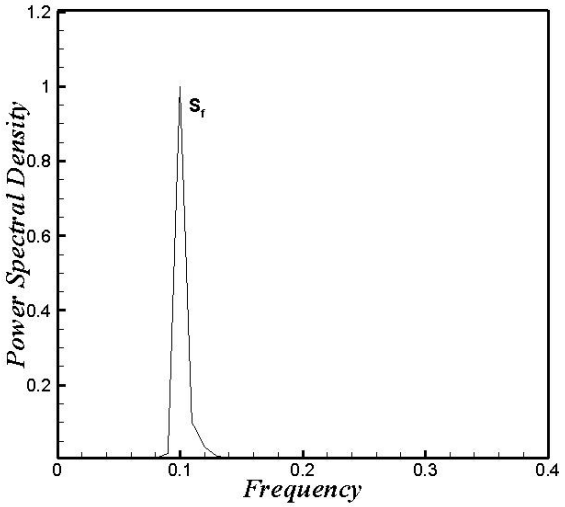

Fig. 4(b) Power Spectra for Re = 200, S_f/S_o = 1.0 and α_m = 0. 5

peak for S_f/S_o = 0.2 for both the values of α_m considered here, but size of the weaker peak is very small for α_m = 2.0. On the other hand, power spectra for S_f/S_o = 1.0 shows only one peak for both the values of α_m considered here. Also, we have observed that there is an increase in the amplitude of fluctuation of both the lift and drag coefficients for S_f/S_o =0.2 and α_m = 2.0 as compared to the case for S_f/S_o = 0.2 and α_m = 0.5. Our computed results show an excellent agreement with those of the computed results of Cheng et al. [5] and Lu and Sato [6]. Our study confirms that the HOC scheme employed by us is a highly efficient and robust one as could be seen from the accurate computation of the complex flow being considered here.

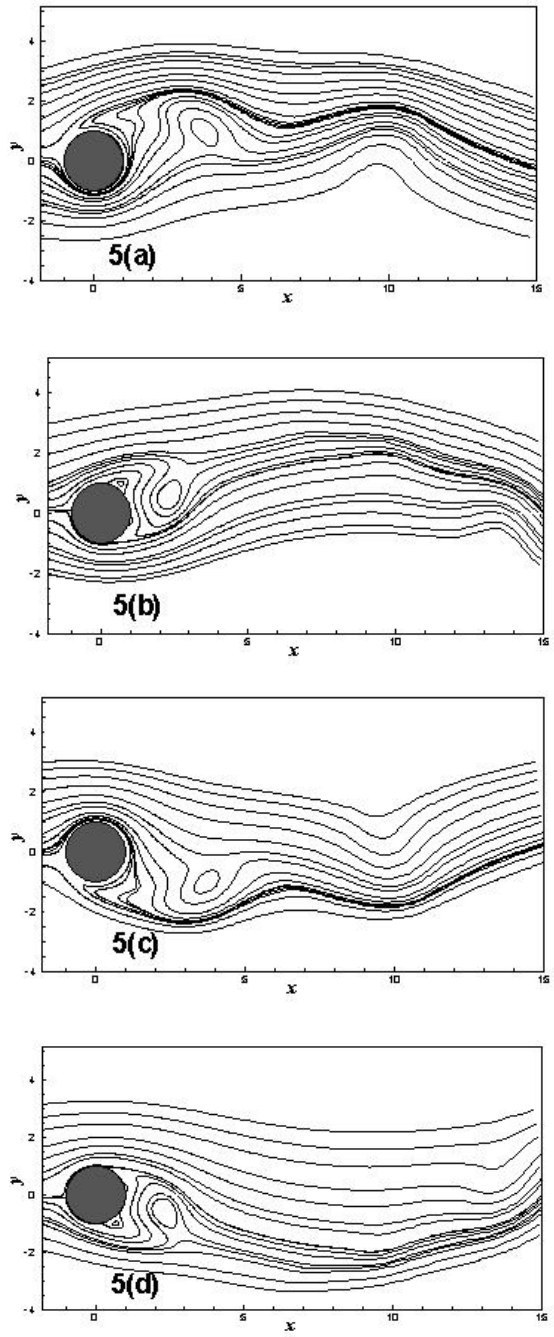

Fig. 5 Streamlines for Re = 200, S_f/S_O = 0.2 and α_m = 2.0, at t = (a) $T_f/4$, (b) $T_f/2$, (c) $3T_f/4$, (d) T_f

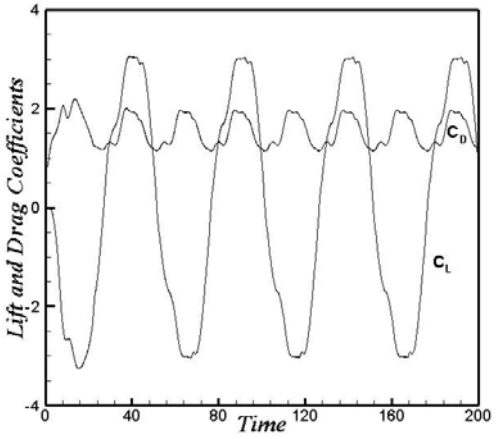

Fig. 6 (a) Lift and Drag coefficients for Re = 200, S_f/S_O = 0.2 and α_m = 2.0

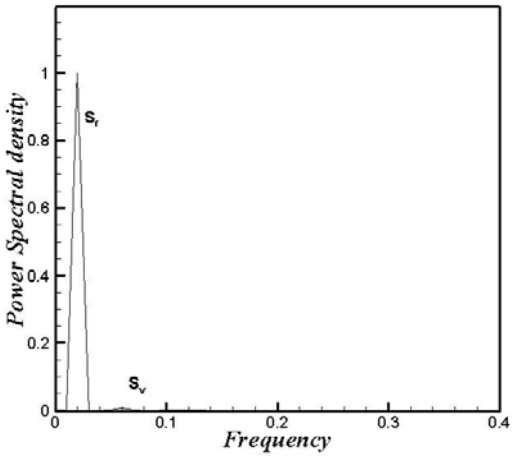

Fig. 6 (b) Power Spectra for Re = 200, S_f/S_O = 0.2 and α_m = 2.0

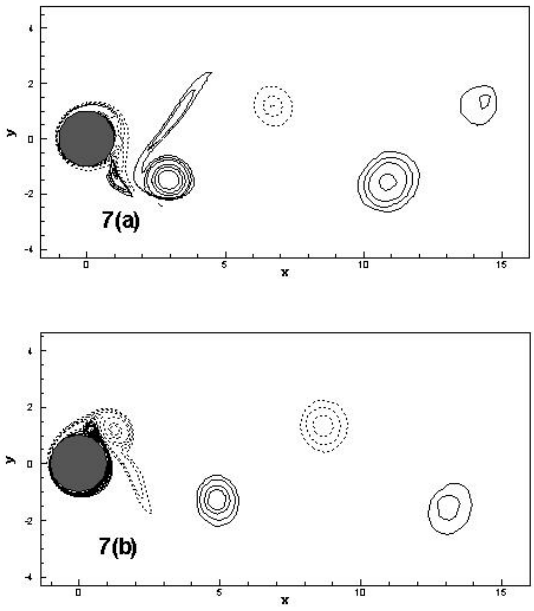

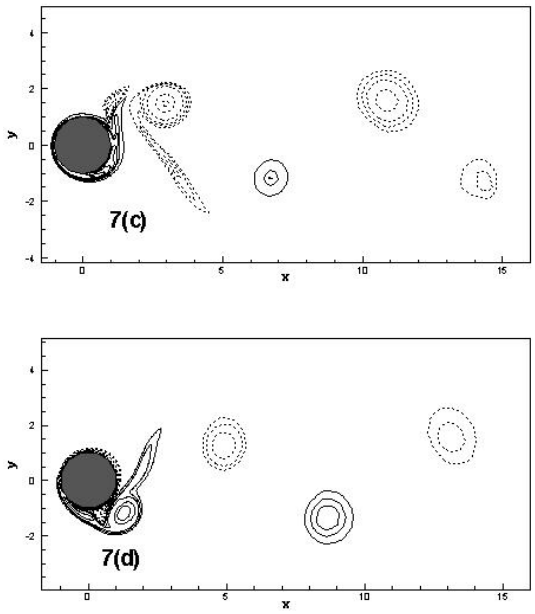

Fig. 7 Vorticity contours for Re = 200, S_f/S_O = 1.0 and α_m = 2.0, at t = (a) $T_f/4$, (b) $T_f/2$, (c) $3T_f/4$, (d) T_f

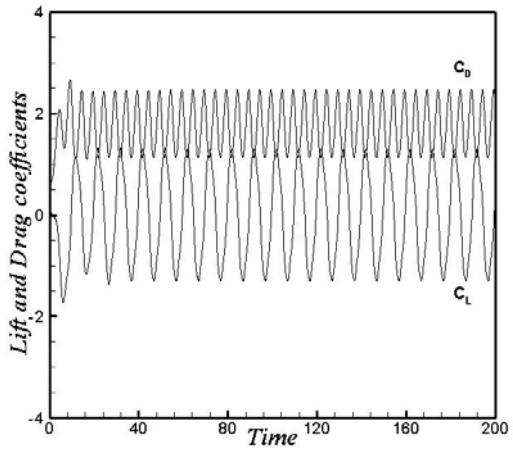

Fig. 8 (a) Lift and Drag coefficients for Re = 200, S_f/S_O = 1.0 and α_m = 2.0

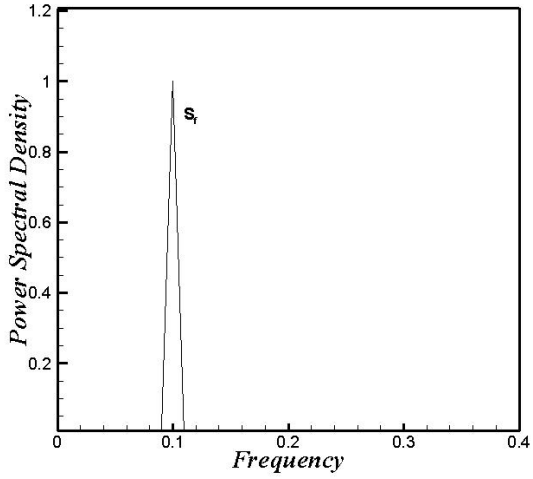

Fig. 8 (b) Power Spectra for Re = 200, S_f/S_O = 1.0 and α_m = 2.0

REFERENCES

[1] J. C. Kalita, A. K. Dass, D. C. Dalal, "A transformation-free HOC scheme for steady-state convection diffusion on non-uniform grids", Int. J. Numer. Methods Fluids, vol. 44, pp. 33-53, 2004.

[2] J. C. Kalita, and R. K. Ray, "A transformation-free HOC scheme for incompressible viscous flows past an impulsively started circular cylinder", J. Computational Physics, vol. 228, pp. 5207-5236, 2009.

[3] R. K. Ray, and J. C. Kalita, "A transformation-free HOC scheme for incompressible viscous flows on non-uniform polar grids", Int. J. Numer. Methods Fluids, vol. 62, pp. 683-708, 2010.

[4] R. K. Ray, "A transformation free HOC scheme for incompressible viscous flow past a rotating and translating circular cylinder", J. Sci. Comput., vol. 46, pp. 265-293, 2011.

[5] M. Cheng, Y. T. Chew, and S. C. Luo, "Numerical investigation of a rotationally oscillating cylinder in a mean flow", J. Fluids and Structures, vol. 15, pp. 981-1007, 2001.

[6] X. Y. Lu, and J. Sato, "A numerical study of flow past a rotationally oscillating circular cylinder", J. Fluids and Structures, vol. 10, pp. 829-849, 1996.